



Novel CRISPR-Cas9 iPSC knockouts for *PCCA* and *PCCB* genes: advancing propionic acidemia research

Emilio M. García-Tenorio^{1,2} · Mar Álvarez¹ · Mónica Gallego-Bonhomme⁵ · Lourdes R. Desviat^{1,2,3,4} · Eva Richard^{1,2,3,4}

Received: 14 December 2024 / Accepted: 25 February 2025
© The Author(s) 2025

Abstract

Propionic acidemia (PA) is a rare autosomal recessive metabolic disorder caused by mutations in the *PCCA* and *PCCB* genes, which encode subunits of the mitochondrial enzyme propionyl-CoA carboxylase (PCC). This enzyme deficiency leads to the accumulation of toxic metabolites, resulting in severe metabolic dysfunction. To create ideal in vitro disease models of PA with isogenic controls and provide a robust platform for therapeutic research, we generated two induced pluripotent stem cell (iPSC) lines with knockout (KO) mutations in the *PCCA* and *PCCB* genes using CRISPR-Cas9 gene editing in a healthy control iPSC line. The KO iPSC cells were successfully established and characterized, confirming the presence of frameshift insertions and deletions in each target gene, as well as the loss of the corresponding transcript, protein expression, and activity. Additionally, the generated iPSC lines exhibit hallmark characteristics of pluripotency, including the potential to differentiate into all three germ layers. Our *PCCA* and *PCCB* KO iPSC models provide a valuable tool for studying the molecular mechanisms underlying PA and hold potential for advancing new therapeutic approaches.

Keywords iPSC · Disease modelling · Propionic acidemia · Isogenic controls · CRISPR-Cas9

Introduction

Propionic acidemia (PA; MIM#606054) is a rare autosomal recessive metabolic disorder caused by mutations in the *PCCA* and *PCCB* genes. These genes encode α (*PCCA*) and β (*PCCB*) subunits of the enzyme propionyl-CoA carboxylase (PCC, E.C.6.4.1.3), which is crucial for the catabolism of certain amino acids and lipids. Mutations in these genes lead to a deficiency in enzyme activity, resulting in the accumulation of toxic metabolites that can cause severe

and life-threatening symptoms, including metabolic acidosis, developmental delay and organ dysfunction [1]. In PA, both the heart and brain can be significantly affected being the principal causes of morbidity and mortality [2]. The most common cardiac complications are QT prolongation, hypertrophy and dilated cardiomyopathy, which can lead to fatal cardiac arrhythmias [3]. Furthermore, patients with PA exhibit a wide range of neurological manifestations, including cognitive impairment, developmental delay and intellectual disability, as well as structural defects, and disorders of neuro-psychomotor development [4]. Early diagnosis and management are crucial to mitigating the damage to these vital organs in individuals with PA. Current therapeutic options are limited, underscoring the need for advanced disease models to better understand PA and explore potential treatments.

Induced pluripotent stem cells (iPSCs) offer a promising platform for modelling genetic diseases, as they can be derived from patient cells and have the ability to differentiate into various cell types [5, 6]. Patient-derived iPSCs may be compared with iPSC lines from healthy individuals used as controls. However, differences in phenotype might result from variations between cell lines rather than from

✉ Eva Richard
eva.richard@uam.es

¹ Centro de Biología Molecular Severo Ochoa UAM-CSIC, Universidad Autónoma de Madrid, 28049 Madrid, Spain

² Instituto Universitario de Biología Molecular, Universidad Autónoma de Madrid, Madrid, Spain

³ Centro de Investigación Biomédica en Red de Enfermedades Raras (CIBERER), ISCIII, Madrid, Spain

⁴ Instituto de Investigación Sanitaria Hospital La Paz (IdiPaz), Madrid, Spain

⁵ Madrid, Spain

the disease-causing variants themselves. In recent years, CRISPR-Cas9-mediated gene-editing technology has been effectively used for gene modification in iPSCs to generate models of inherited diseases [7]. The creation of isogenic pairs of disease-specific and control iPSCs, differing solely at the disease-causing mutation, has been employed to minimize variability, allowing the identification of disease-relevant differences in monogenic disorders [8]. In addition, parallel differentiation of these isogenic cell lines into relevant cell types facilitates detailed phenotypic analysis of cellular pathologies specific to the disease [7].

In this study, we utilized CRISPR-Cas9 to generate two knockout (KO) iPSC lines for the *PCCA* and *PCCB* genes from a healthy control iPSC line. These genetically modified iPSCs provide a valuable isogenic system to study the molecular and pathophysiologic mechanisms of PA and represent a versatile tool for investigating potential therapeutic interventions in this rare disease.

Materials and methods

Cell line and culture

Human iPSC control line SCTi003-A (StemCell™ Technologies #200–0511, Vancouver, BC, Canada), a hiPSC line derived from peripheral blood mononuclear cells of a healthy female donor, was used in this work. iPSC cells were cultured in 60 mm tissue culture dishes coated with Matrigel (hESC-qualified matrix, Corning, New York, NY, USA), using mTESR™ Plus medium (StemCell™ Technologies) at 37 °C with 5% CO₂ and 20% O₂, with medium changes every other day. The iPSCs were passaged every four days using ReleSR™ (StemCell™ Technologies) or StemPro Accutase (Gibco, Waltham, MA, USA) and 10 μM Rock inhibitor (StemCell™ Technologies) at a 1:3–1:5 splitting ratio.

CRISPR-Cas9-mediated gene KO

The online tools available at <https://bioinfogp.cnb.csic.es/tools/breakingcas/> and <http://crispor.gi.ucsc.edu/> were used to design guides with high specificity for *PCCA* and *PCCB* target sites while minimizing predicted off-targets located in genomic regions (Table 1). On the day of nucleofection, 2×10^5 cells (80% confluency and passage 4) were nucleofected using a Neon Electroporation Kit (Invitrogen, #MPK1025, Waltham, MA, USA) and the Neon Transfection System (Invitrogen), according to provider's instructions. Ribonucleoprotein (RNP) complexes were formed by the combination of 45 pmol of Cas9 (*Streptococcus pyogenes*, Integrated DNA Technologies (IDT), Newark, NJ, USA) and 55 pmol of RNA duplex constituted by tracrRNA

and RNA guide (IDT); and with 55 pmol of enhancer (IDT). Cells were transferred into a single well of a Matrigel-coated 12-well plate and cultured in mTESR™ Plus medium. Several days after nucleofection, the cells were transferred to Matrigel-coated 60 mm dishes in mTESR™ Plus medium. Cells were then sorted using a FACS Aria Fusion (BD Biosciences, Franklin Lakes, NJ, USA) into Matrigel-coated 96-well plates with mTESR™ Plus medium supplemented with 1X CloneR (StemCell™ Technologies) for clonal expansion.

PCC enzymatic assay

PCC activity was assayed by measuring the enzyme-dependent incorporation of radiolabelled bicarbonate into non-volatile products, as previously described [9].

Karyotype analysis

Cells were exposed to 10 μg/ml Colcemid® Solution (Irvine Scientific, Santa Ana, CA, USA) for 3 h at 37 °C, then dissociated using accutase, treated with a hypotonic solution, and fixed with Carnoy's fixative in preparation for karyotype analysis. A minimum of 20 metaphase cells were analyzed. Karyotype analysis was performed by the Molecular Cytogenetics and Genome Editing Unit from Centro Nacional de Investigaciones Oncológicas (CNIO, Madrid, Spain).

DNA extraction and PCR mismatch

Genomic DNA was extracted from iPSCs using QIAamp DNA Mini Kit (Qiagen, Venlo, The Netherlands) following the manufacturer's recommendations. Editing was verified by PCR mismatch using 100 ng of DNA from the cell population, the specific primers for target knockout analysis (Table 1), and the Supreme NZYTaq II 2× Green Master Mix (NZYTech, Lisbon, Portugal).

Sequencing

PCR products were cloned in pGEM®-T Easy Vector System I (Promega Corporation, Madison, WI, USA). Plasmid DNA was purified using NZYMiniprep Kit (NZYtech) and was subjected to Sanger sequencing (Macrogen, Seoul, South Korea). At least 20 colonies were sequenced. Deep sequencing was performed using amplicons generated in a first PCR with fusion primers containing a specific sequence plus a common tag (Table 1). Libraries preparation and sequencing were carried out at Fundación Parque Científico de Madrid (Campus Cantoblanco, Madrid, Spain) under protocols developed and optimized for next-generation amplicon sequencing. For off-target analysis, PCR products

Table 1 Primers and RNA guides used in the study

	Target	Oligonucleotides (5'–3')*
Target sequences (gRNA)	<i>PCCA</i> exon 5	gRNA: UUCAUUCAGACUCACAGCTT
	<i>PCCB</i> exon 5	gRNA: AUGGACCAGGCCAUACGGU
Target knockout analysis	<i>PCCA</i> exon 5	Fwd: GTCTCCTCAGGTTTCATGTGA Rev: AGTAGATAGATTCATTCAGACTCACAG
	<i>PCCB</i> exon 5	Fwd: CAGATCATGGACCAGGCCATAAC Rev: GAGGAGAGTTGGGAGAAGCTCTGGC
Sanger sequencing	<i>PCCA</i> exon 5	Fwd: GTCTCCTCAGGTTTCATGTGA Rev: AGTAGCGAATTCGACCACAT
	<i>PCCB</i> exon 5	Fwd: GGGAGTGAAACCAGTGTTACTGCC Rev: GAGGAGAGTTGGGAGAAGCTCTGGC
Next generation sequencing	<i>PCCA</i> exon 5	Fwd: ACACTGACGACATGGTTCTACAGTCTCCTCAGGTTTCATGTGA Rev: TACGGTAGCAGAGACTTGGTCTAGTAGCGAATTCGACCACAT
	<i>PCCB</i> exon 5	Fwd: ACACTGACGACATGGTTCTACAGGGAGTGAAACCAGTGTTACTGCC Rev: TACGGTAGCAGAGACTTGGTCTGAGGAGAGTTGGGAGAAGCTCTGGC
RT-PCR	<i>PCCA</i> exon 2–7	Fwd: GTGTCCCGTAATCTTGGTTC Rev: CAGGGATTGTATTAACCTCTGCTT
Quantitative PCR	<i>PCCA</i> exon 1–4	Fwd: GGACCCTGAAGCATGTTCTGTAC Rev: TAACCCGACATGCAATTTCTCC
	<i>PCCB</i> exon 1–3	Fwd: GCACAAGCGAGGAAAGCTAAC Rev: CGCTGTCTCCAGGAAACTTATTC
Off-target analysis <i>PCCA</i>	<i>LINC02869</i>	Fwd: GCAAATCCGCAACATCAGC Rev: AGTGAGGAGGCACAGCAAC
	<i>STX11</i>	Fwd: ACCAAGACCCCATCTTCTGTG Rev: CATTTCACCCACTGCCTGG
	ENSG00000250971	Fwd: GGACTGAGACTGAACCCTTGG Rev: CCACCCTGAGGCACACTAAAG
	AC064870.5	Fwd: GGCTGAGTCCCTGTGAAGAAG Rev: CTTATTCATGGTCCCACAGCAG
Off-target analysis <i>PCCB</i>	<i>SLC7A14-AS1</i>	Fwd: AAAGCAGTGAGCCAGTGGG Rev: TTCCTGTGAAAGCGGTGG
	AC117526.2	Fwd: AGGTGGAAGTTTGCTGAGTGG Rev: AATGCTCTTACTGGCTGATGC
	AL034431.16	Fwd: ACTCTTGCTCTCAGCCCATTG Rev: CACCTCAGACTACTCTGGCAC
	<i>SLC2A13</i>	Fwd: CCTGACCTCAAGTATCCACCC Rev: GTGGCTGTTCCAAACAAGGTC
Mycoplasma detection	Mycoplasma species	Forward primers: CGCCTGAGTAGTACGTTTCGC CGCCTGAGTAGTACGTTTCGC TGCCTGGGTAGTACATTTCGC TGCCTGAGTAGTACATTTCGC CGCCTGAGTAGTATGCTTCGC CACCTGAGTAGTATGCTTCGC CGCCTGGGTAGTACATTTCGC Reverse primers: GCGGTGTGTACAAGACCCGA GCGGTGTGTACAAAACCCGA GCGGTGTGTACAAGACCCGA

*gRNA RNA guide, Fwd Forward, Rev Reverse

were purified using E.Z.N.A Cycle Pure kit (Omega Bio-Tek, Norcross, GA, USA) before Sanger sequencing.

RNA extraction, RT-PCR and RT-qPCR

To assess the splicing effects in the *PCCA* KO cell line, total RNA was isolated using TRIzol® Reagent (Life Technologies, Waltham, MA, USA), and 1 µg of RNA was retrotranscribed using NZY First-Strand cDNA Synthesis kit (NZY Tech). RNA from the unedited iPSC line was used as a control. PCR was performed using the primers hybridizing to exons 2 and 7 of the *PCCA* gene (Table 1), and FastStart Taq DNA polymerase (Roche Diagnostics GmbH, Mannheim, Germany). PCR products corresponding to transcripts were separated on an agarose gel and purified using a QIAquick gel extraction kit (Qiagen) before Sanger sequencing.

To assess the effect of gene KO on their respective target mRNA levels, cDNA was obtained by retrotranscription of 500 ng of total RNA as described above. *PCCA* and *PCCB* were then amplified with specific primers designed upstream of the edition site (Table 1), using PerfeCTa SYBR Green FastMix (Quanta Biosciences, Beverly, MA, USA) in a CFX Opus 384 real-time PCR system (Bio-Rad, Hercules, CA, USA) following the manufacturer's instructions. Data were analysed using Bio-Rad CFX Maestro software, and

relative quantification to the wild-type iPSC line was performed according to $2^{-\Delta\Delta CT}$ method, using *GAPDH* as an endogenous control.

Immunoblot analysis

Protein extracts were prepared from frozen cell pellets through a freeze–thaw lysis process using a buffer containing Tris–HCl pH 7.4, 10% glycerol, 150 mM NaCl, 0.1% Triton X-100, and protease and phosphatase inhibitor cocktail (Sigma-Aldrich, St. Louis, MO, USA). Lysates were then centrifuged for 10 min at 4 °C, after which the supernatant was collected, and protein concentration was measured using the Bradford method (Bio-Rad). 40 µg of protein from each sample were loaded onto 4–12% NuPAGE™ Precast Gels (Invitrogen). After electrophoresis, proteins were transferred to a nitrocellulose membrane in an iBlot Gel transfer device (Invitrogen), then incubated with the primary antibodies at 4 °C overnight (Table 2), and subsequently incubated with the secondary antibodies at room temperature for 1 h (Table 2). GAPDH was used as a loading control. Enhanced chemiluminescence reagent (ECL, GE Healthcare, Chicago, IL, USA) and SuperSignal™ West Femto Maximum Sensitivity Substrate (Thermo Fisher Scientific, Waltham, MA, USA) were used for protein detection.

Table 2 Antibodies used in the study

	Antibody	Dilution	Company Cat# and RRID
For immunocytochemistry/flow cytometry			
Pluripotency markers	Mouse IgG anti-Oct4	1:60	Santa Cruz Cat# sc-5279, AB_628051
	Rabbit IgG anti-Sox2	1:100	Fisher Thermo Scientific Cat# PA1-16968, AB_2195781
	Goat IgG anti-Nanog	1:25	R&D Cat# AF1997, AB_355097
	Rat IgM anti-SSEA3	1:3	Hybridoma Bank Cat# MC-631, AB_528476
	Mouse IgG anti-SSEA4	1:3	Hybridoma Bank Cat# MC-813-70, AB_528477
	Mouse IgM anti-Tra1-60	1:200	Millipore Cat# MAB4360, AB_2119183
Differentiation markers	Mouse IgM anti-Tra1-81	1:200	Millipore Cat# MAB4381, AB_177638
	Rabbit IgG anti- α -1-fetoprotein	1:400	Dako Cat# A0008, AB_2650473
	Mouse IgG anti- α -smooth muscle actin	1:400	Sigma-Aldrich Cat# A5228, AB_262054
Secondary antibodies	Mouse IgG anti- β -III-Tubulin Tuj1	1:500	Covance Cat# MMS-435P, AB_231377
	Alexa 555 Donkey anti-mouse IgG	1:200	Thermo Fischer Cat# A-31570, AB_2536180
	Alexa 488 Donkey anti-Rabbit IgG	1:200	Thermo Fischer Cat# A-31572, AB_162543
	Alexa 647 Donkey anti-Goat IgG	1:200	Thermo Fischer Cat# A-21447, AB_2535864
	Alexa 488 Goat anti-Rat IgM	1:200	Thermo Fischer Cat# A-21212, AB_2535798
	Alexa 647 Goat anti-Mouse IgM	1:200	Thermo Fischer Cat# A-21238, AB_2535807
	Cy3 Donkey anti-Mouse IgM	1:200	Jackson Cat# 715-165-140, AB_2340812
	Alexa 647 Goat anti-mouse IgG	1:600	Thermo Fischer Cat# A-21235, AB_2535804
For Western Blot	APC Rat anti-mouse APC	1:150	BD Pharmingen Cat# 550676, AB_398464
	Mouse IgG anti-PCCA	1:500	Santa Cruz Cat# sc-374341, AB_10987856
	Mouse IgG anti-PCCB	1:500	Santa Cruz Cat# sc-393929
	Mouse IgG anti-GAPDH	1:5000	Abcam Cat# ab8245, AB_2107448
	Goat anti-Mouse	1:2000	Santa Cruz Biotechnology Cat# sc-2031, AB_631737

Immunostaining

iPSCs were seeded onto matrigel-coated 15 μ -Slide 8 well culture plates (Ibidi, GmbH, Gräfelting, Germany), fixed with Formaline Solution 10% (Sigma-Aldrich), and stained with anti-OCT4/NANOG/SOX2/SSEA-3/SSEA-4/TRA-1-60 and TRA-1-81 at 4 °C overnight using the dilutions previously described [10]. Tris-buffered saline was used for washing, blocking and antibody incubation solutions supplemented with Triton-X100 (Sigma-Aldrich) (Nuclear markers: 0.1% for washes and 0.3% for blocking and antibody incubation solutions) and Tween-20 (Merck Millipore, Burlington, MA, USA) (Surface markers: 0.2% for washes and 0.4% for blocking and antibody incubation solutions). Blocking and antibody incubation solutions were also supplemented with 3% Donkey Serum (Sigma-Aldrich). After several washes, cells were labelled with secondary antibodies for 2 h at 37 °C, followed by 30 min at room temperature. For nucleus staining DAPI (Invitrogen, 1:10,000) was used. Images were obtained using a Nikon A1R fluorescence microscope. Antibodies details are in Table 2.

Flow cytometry analysis

The pluripotency markers SSEA-4, TRA-1-60, and TRA-1-81 were also examined by flow cytometry, as detailed in [10], using a BD FACSCanto™ A instrument (BD Biosciences), FACSDiva and FlowJo v10.10 software program. Unstained iPSCs and matching isotype antibodies served as negative controls to eliminate non-specific fluorescence data.

In vitro three-germ-layer differentiation assay

Embryoid body (EB) formation was applied by plating the dissociated cells onto 96-well v-bottom, low attachment plates (Deltalab, Barcelona, Spain). Emerging EB were replated on matrigel-coated 15 μ -Slide 8 well culture plates (Ibidi) for another 18 days with different mediums as described [10]. Cells were fixed with Formaline Solution 10% and stained with endodermal (α -1-Fetoprotein, AFP), mesodermal (α -Smooth muscle actin, SMA) and ectodermal (β -III-Tubulin Tuj1, TUJ1) differentiation markers (Table 2).

Short tandem repeat (STR) analysis

DNA fingerprinting analysis was conducted using the Amp-FLSTR® Identifiler® PCR Amplification Kit (Thermo Fisher Scientific). For this process, 1 ng of DNA was used to evaluate highly polymorphic regions containing short tandem repeats by amplifying the following markers: D7S820, CSF1P0, Th01, D13S317, D16S539, vWA, TPOX, D5S818, and Amelogenin for determining sex. Samples were analyzed on a 3730 DNA Analyzer (Applied Biosystems, Foster

City, CA, USA), and data processing was done using GeneMapper® v4.0 software at the Parque Científico de Madrid, Campus Moncloa, UCM, Madrid, Spain.

Mycoplasma detection

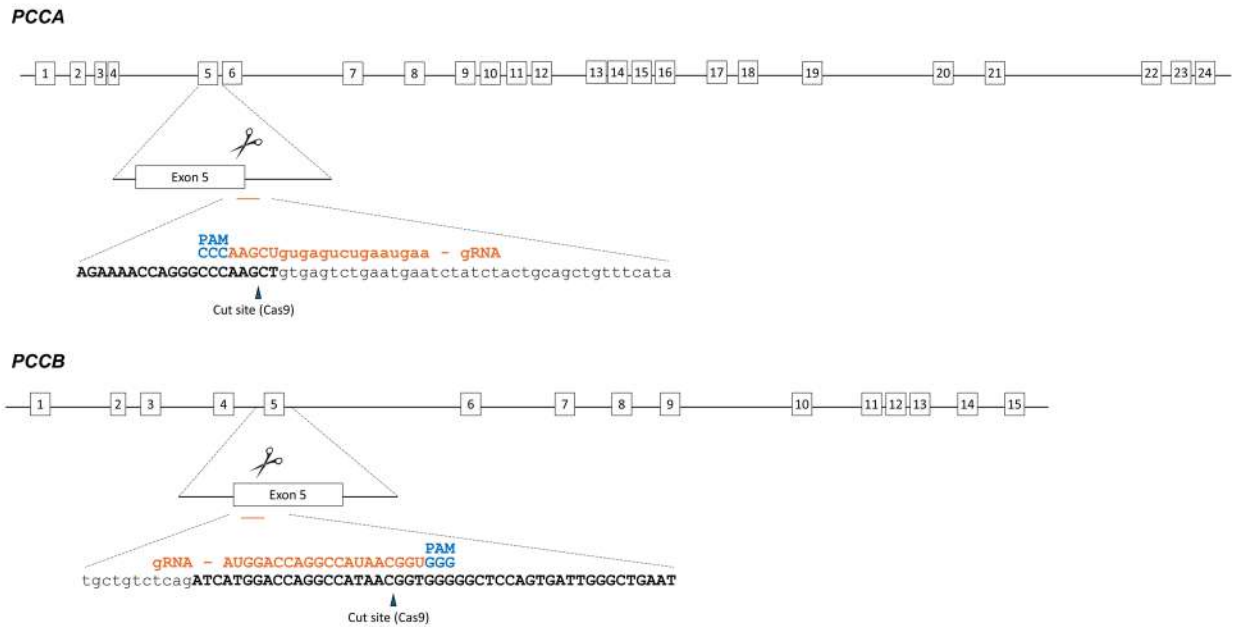
Mycoplasma test was performed using the PCR method [11]. A positive sample with mycoplasma was used as a control.

Results

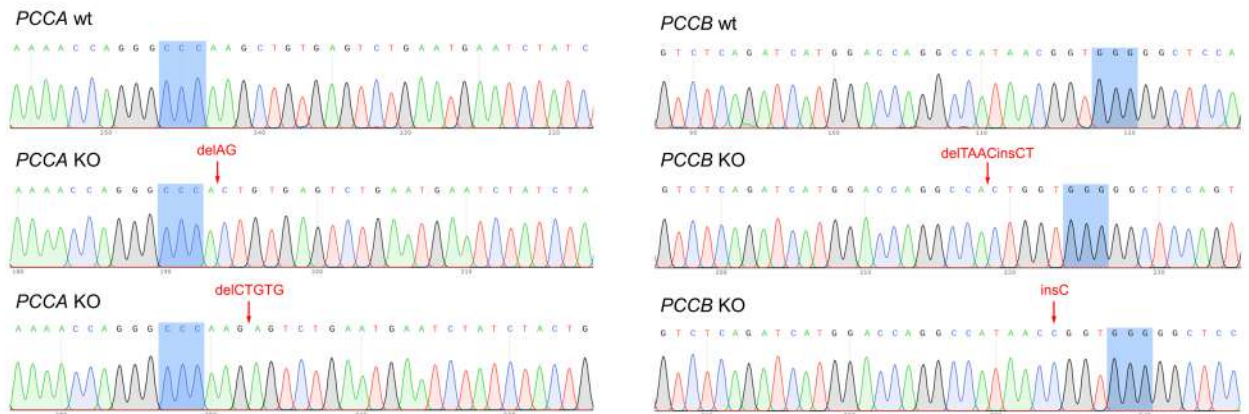
Generation of *PCCA* and *PCCB* KO iPSC lines

To generate KO iPSC lines for the *PCCA* and *PCCB* genes, we designed specific guides targeting key regions within each gene. For both cases, the guides were directed at exon 5, an essential region for the proper function of the encoded proteins (Fig. 1A). The guides were selected based on their predicted on-target efficiency and low off-target potential, using the CRISPOR and Breaking-Cas design tools. After nucleofection with CRISPR-Cas9 and sgRNA RNP complexes, up to 12 iPSC colonies were manually picked and screened for insertion-deletions (indels) within the target regions using PCR mismatch, revealing the presence of edition in all of them. Subsequently, cell sorting and expansion of individual clones was performed to ensure the isolation of pure homogeneous clones. The mutations in the selected clones were identified by Sanger sequencing after subcloning to separate the two alleles (Fig. 1B), and the results were further confirmed by deep sequencing of each region (data not shown). Our sequencing results revealed the presence of biallelic frameshift mutations within the target exons of both *PCCA* and *PCCB* genes. Specifically, in the *PCCA* KO iPSC line, we identified two frameshift-causing mutations: 2-bp (c.411_412del) and 5-bp (c.413_414 + 3del) deletions. The c.411_412del variant introduces a premature stop codon 30 amino acids downstream of the edited site (p.(Gln137Hisfs*30)), while c.413_414 + 3del disrupts the 5' splice site of exon 5, predictably causing a splicing defect. This splicing alteration was confirmed by RT-PCR and sequencing of the transcript, which revealed the inclusion of 40 bp of the intronic sequence following the deletion (r.413_414delins40), due to the activation of a cryptic splice site. This alteration was also predicted to result in a premature stop codon (p.(Ala138Glu fs*4)). From the edited *PCCB* iPSC clones, we selected a compound heterozygous clone in which one allele carries a 1 bp insertion (c.448_449insC) and the other allele a 4 bp deletion with a 2 bp insertion (c.446_449delinsCT), both resulting in frameshifts and premature stop codons at residues 10 (p.(Val151Glyfs*10)) and 11 (p.(Ile149Thrfs*11)) downstream of the edition, respectively.

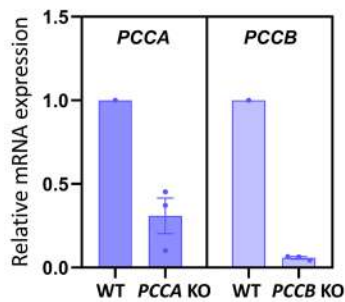
A



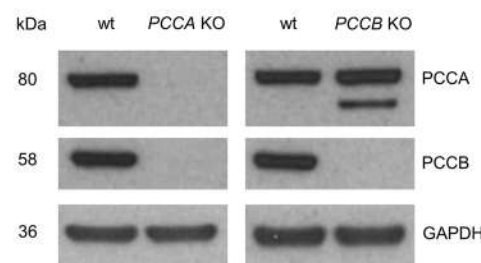
B



C



D



E

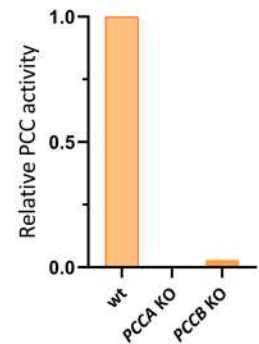


Fig. 1 Generation of the *PCCA* and *PCCB* KO iPSC lines. **A** Schematic representation of *PCCA* and *PCCB* genes. The specific RNA guides are indicated in both genes (orange) with their respective PAM sequences (blue). **B** Sanger sequencing results after subcloning both alleles of the generated KO iPSC lines. PAM sequences are highlighted in blue. **C** RT-qPCR for *PCCA* and *PCCB* genes in their respective KO iPSC lines compared to the wild-type (wt). The relative quantification data presented include the mean and standard error of mean for three biological replicates. **D** Western Blot against *PCCA* and *PCCB* proteins in the wild-type iPSC line (wt) and KO iPSC lines. GAPDH was used as a loading control. **E** Histogram representation of PCC activity in the wild-type iPSC line (wt) and KO iPSC lines

These mutations in both genes were predicted to be disease-causing by Mutation Taster (<http://www.mutationtaster.org/>). Specifically, the mutations lead to the absence of part of the biotin carboxylase domain in the *PCCA* gene, and of the carboxyl transferase domain in the *PCCB* gene, respectively. Our results showed a reduction in *PCCA* and *PCCB* mRNA levels in the respective KO iPSCs (Fig. 1C), which may be due to nonsense-mediated mRNA decay, triggered by the premature stop codons generated by the editing process. If any transcripts are produced, an unstable truncated protein would be generated and rapidly degraded, as confirmed by Western Blot analysis and PCC activity measurement. These assays revealed a complete absence of protein expression (Fig. 1D) and enzymatic activity (Fig. 1E) in both *PCCA* and *PCCB* KO iPSC lines, confirming the successful generation of the KO lines. In the *PCCA* KO iPSC line we observed a loss of both *PCCA* and *PCCB* protein expression, as expected. This occurs because, although the *PCCB* protein is expressed, it is unstable and prone to degradation in the absence of the *PCCA* subunit [12]. However, in the *PCCB* KO line, *PCCA* is still expressed in the absence of *PCCB*, although a smaller degradation product is also observed (Fig. 1D).

Additionally, Sanger sequencing analysis revealed the absence of off-target events in the top four predicted off-target sites for both clones (Fig. S1).

Characterization of *PCCA* and *PCCB* KO iPSC lines

We performed a comprehensive characterization of the KO clones for the *PCCA* and *PCCB* genes to confirm their genomic integrity and evaluate their pluripotency potential (Fig. 2). Both KO iPSC lines exhibited typical stem cell-like morphology, forming colonies with tightly packed cells that had large nucleus-to-cytoplasm ratios and prominent nucleoli (Fig. 2A). Karyotyping was conducted to assess the chromosomal integrity of each clone and verify that no cytogenetic abnormalities were introduced during the gene editing process. The cell lines maintained a normal molecular karyotype (46, XX) (Fig. 2B).

Immunofluorescence staining demonstrated robust expression of pluripotency markers in both iPSC lines. Nuclear markers OCT4, SOX2 and NANOG, as well as surface markers SSEA-3, SSEA-4, TRA-1-60 and TRA-1-81 were all highly expressed (Fig. 2C). Flow cytometry analysis further confirmed that over 72% of cells expressed the surface markers SSEA-4, TRA-1-60 and TRA-1-81 across the cell populations (Fig. 2D).

Additionally, the functional pluripotency of the iPSCs was evaluated through directed differentiation into the three germ layers. This was achieved by using EB formation, followed by immunocytochemical analysis of lineage-specific markers: AFP for endoderm, SMA for mesoderm and TUJ1 for ectoderm (Fig. 2E). Positive expression of all three markers confirmed the strong differentiation potential of the *PCCA* and *PCCB* KO iPSC lines, indicating that the gene knockouts did not impair their ability to differentiate into the three germ layers.

Finally, STR profiling at 9 loci validated the cell identity of the *PCCA* and *PCCB* KO iPSCs by matching them to their parental wild-type cells (Fig. S2A). Rigorous mycoplasma testing confirmed that both cell lines were free of contamination, preserving the integrity of the experimental conditions and results (Fig. S2B).

Discussion

Over the last decade, the generation of iPSCs has revolutionized biomedical research, enabling scientists to explore previously inaccessible aspects of human biology, such as early developmental stages, cellular differentiation, and the progression of genetic diseases at a cellular level. This technology has also paved the way for advancements in personalized medicine and regenerative therapies by allowing the creation of patient-specific cell lines [13].

Previously, we generated two iPSC lines from patient-derived fibroblasts with defects in the *PCCA* and *PCCB* genes [10, 14], as well as an isogenic *PCCB*-corrected cell line using CRISPR-Cas9 gene editing [15]. Working with patient-derived iPSCs and generating appropriate isogenic controls using CRISPR-Cas9 technology poses significant challenges, particularly in the case of *PCCA*-deficient patients in which large genomic deletions are frequent [16]. These PA iPSC lines initially provided an essential platform for dissecting the molecular mechanisms underlying the disease, especially in tissues highly affected by PA deficiency, such as the heart. In patient-derived iPSC cardiomyocytes, we observed upregulation of cardiac-enriched miRNAs and alterations in key signaling pathways, including increased cardiac damage markers and cardiac ion channels, oxidative stress, reduced mitochondrial respiration, impaired autophagy, and lipid accumulation [17, 18].

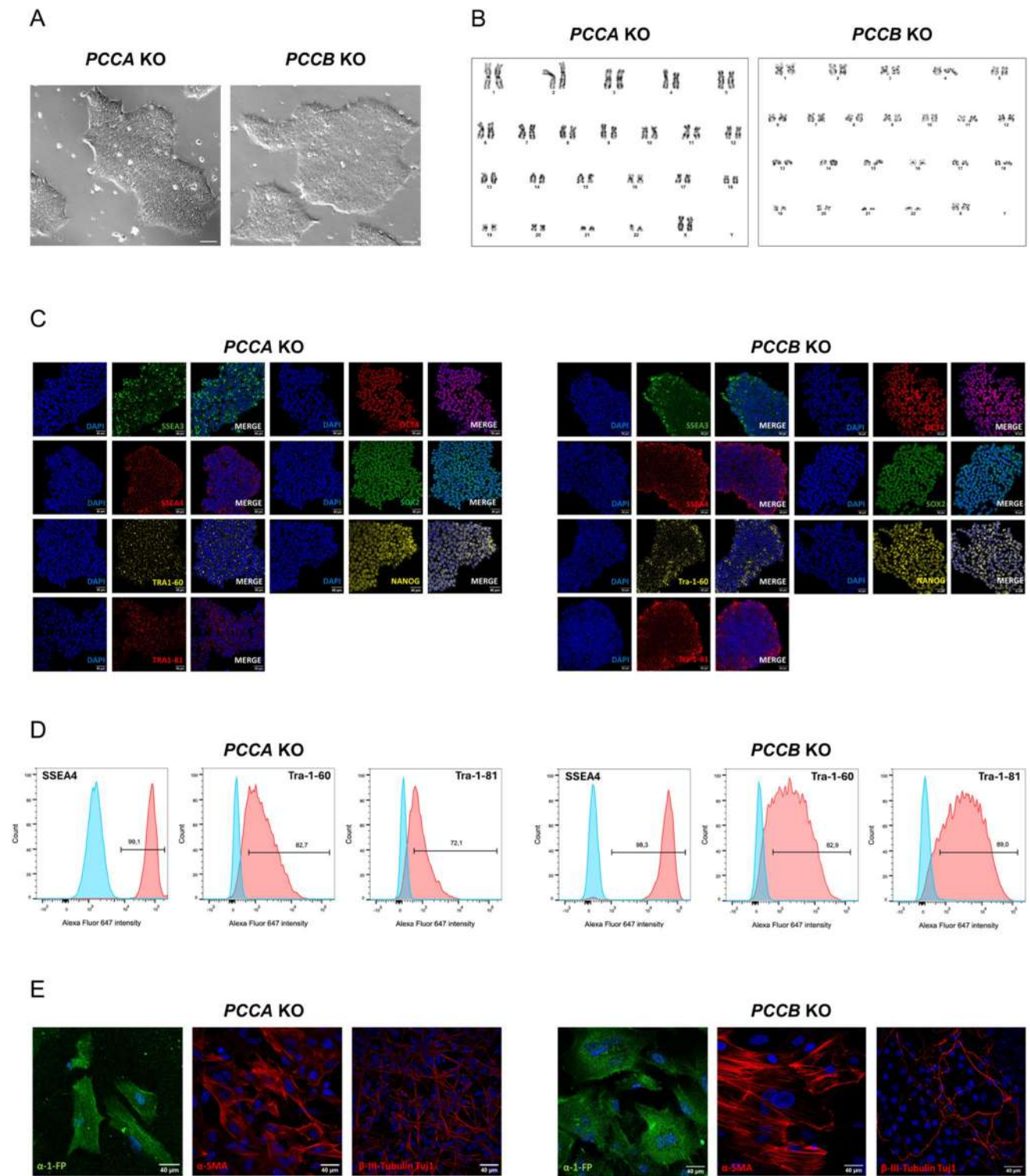


Fig. 2 Characterization of the *PCCA* and *PCCB* KO iPSC lines. **A** Representative phase contrast images of iPSC colonies in both KO iPSC lines (scale bar 40 μ m). **B** Representative G-banding karyotype images of normal 46, XX for both cell lines. **C** Immunofluorescence analysis for OCT4/NANOG/SOX2/SSEA-3/SSEA-4/TRA-1-60 and

TRA-1-81 pluripotency markers (scale bar 40 μ m). **D** Flow cytometry analysis for SSEA-4/TRA-1-60 and TRA-1-81 surface pluripotency markers. **E** In vitro differentiation analysis by immunofluorescence for AFP, SMA and TUJ1 proteins (scale bar 40 μ m)

In this study, we focused on creating isogenic iPSC lines deficient in *PCCA* and *PCCB* genes, successfully generating two KO iPSC lines from a control line. The precision of the knockout strategy, demonstrated by the introduction of out-of-frame indels within exon 5, led to the generation of premature stop codons in both genes, resulting in a loss of the corresponding transcript, protein expression, and function, as confirmed by *in silico* predictions and experimental validation. The generated KO iPSC lines exhibit genomic integrity and maintain pluripotency characteristics. This not only highlights the effectiveness of CRISPR technology for creating disease-relevant models [19, 20] but also underscores its potential for investigating PA with isogenic disease models.

PA patients suffer irreversible cerebral complications due to the currently limited therapeutic options. Brain imaging studies in PA patients have revealed a range of abnormalities, including bilateral basal ganglia damage, generalized brain atrophy, delayed myelination, white matter changes, cerebral atrophy, intracranial and cerebellar hemorrhage, and medullary lesions [4]. The exact pathophysiological mechanism by which PA causes brain complications remains unclear [21], although several mechanisms involving the accumulation of propionate and its toxic metabolites have been proposed. These include disruptions in signaling pathways like cAMP and type I protein kinase, altered phosphorylation of the cytoskeletal protein, glial fibrillary acidic proteins and vimentins, inhibited lipid biosynthesis (potentially causing demyelination), impaired ganglioside production, oxidative stress, mitochondrial dysfunction, and altered gene expression in neuronal and glial cells [4, 22]. To our knowledge, relevant cellular models of PA for studying neurological alterations have not been described to date, with iPSCs representing a promising tool for their generation, as has been demonstrated for other neurometabolic disorders, such as tyrosine hydroxylase deficiency [23].

Moving forward, our next goal is to develop cerebral organoids from these KO iPSCs. Organoids provide a unique opportunity to mimic the 3D architecture and cellular diversity of the human brain, offering deeper insights into disease mechanisms [24]. By developing these cerebral organoids, we aim to advance our understanding of the neurological and biological complexities associated with PA and investigate potential differences between the *PCCA* and *PCCB*-affected cells, given that *PCCB* has been associated with various neurodevelopmental and neuropsychiatric disorders such as autism [25, 26] and schizophrenia [27], while the presence of autistic features in *PCCA* deficient patients is far less common [25, 26].

In conclusion, the use of the wild-type line alongside the *PCCA* and *PCCB* KO iPSC lines provides a robust platform for future research aimed at understanding the pathophysiology of PA disease. These models also represent a critical

step toward developing novel therapeutic strategies, as they will be instrumental for investigating potential treatments, particularly in gene-specific contexts.

Supplementary Information The online version contains supplementary material available at <https://doi.org/10.1007/s13577-025-01193-z>.

Acknowledgements We particularly thank Leonardo Beccari for his assistance with the nucleofection assays, the Optical and Confocal Microscopy and the Flow Cytometry Units from Centro de Biología Molecular Severo Ochoa (CBMSO, Madrid, Spain); Molecular Cytogenetics and Genome Editing Unit from Centro Nacional de Investigaciones Oncológicas (CNIO, Madrid, Spain) and Parque Científico de Madrid (Madrid, Spain).

Author contributions Emilio M. García-Tenorio: Visualization, Methodology, Investigation, Formal analysis. Mar Álvarez: Visualization, Methodology, Investigation, Formal analysis. Mónica Gallego-Bonhomme: Methodology, Formal Analysis. Lourdes R. Desviat: Writing—review & editing, Resources, Funding acquisition, Conceptualization. Eva Richard: Writing—review & editing, Writing—original draft, Supervision, Resources, Investigation, Funding acquisition, Conceptualization. All authors read and approved the final version of the manuscript.

Funding Open Access funding provided thanks to the CRUE-CSIC agreement with Springer Nature. This research was funded by Grant PAF113 from the Propionic Acidemia Foundation; Grant from Fundación Ramón Areces (XX National Call 2020) and by grant PID2022-137238OB-100 funded by MICIU/AEI/<https://doi.org/10.13039/501100011033/> and by ERDF A way of making Europe. EMGT is a PhD student funded by the FPU program (grant FPU22/03244). Centro de Biología Molecular Severo Ochoa receives an institutional grant from Fundación Ramón Areces and is a Severo Ochoa Center of Excellence (MICIN, Award CEX2021-001154-S).

Data availability Data will be made available on request.

Declarations

Ethical approval The study was conducted in accordance with the Declaration of Helsinki and approved by the Ethics Committee of the Autonomous University of Madrid (project identification code CEI-134-2830; date of approval: 3 November 2023); and by the authorization of “Dirección General de Investigación Sanitaria y Documentación”, Community of Madrid (date of approval: 19 February 2024).

Informed consent Not applicable.

Conflict of interest The authors declare that they have no conflict of interest.

Open Access This article is licensed under a Creative Commons Attribution 4.0 International License, which permits use, sharing, adaptation, distribution and reproduction in any medium or format, as long as you give appropriate credit to the original author(s) and the source, provide a link to the Creative Commons licence, and indicate if changes were made. The images or other third party material in this article are included in the article's Creative Commons licence, unless indicated otherwise in a credit line to the material. If material is not included in the article's Creative Commons licence and your intended use is not permitted by statutory regulation or exceeds the permitted use, you will need to obtain permission directly from the copyright holder. To view a copy of this licence, visit <http://creativecommons.org/licenses/by/4.0/>.

References

- Fenton WA, Gravel RA, Rosenberg LE. Disorders of propionate and methylmalonate metabolism. In: Scriver CR, Beaudet AL, Sly W, Valle D, editors. *The metabolic and molecular bases of inherited disease*. 8th ed. New York: McGraw-Hill; 2001. p. 2165–90.
- Galarreta Aima CI, Shchelochkov OA, Jerves Serrano T, Venditti CP. Propionic acidemia. In: Adam MP, Feldman J, Mirzaa GM, Pagon RA, Wallace SE, Amemiya A, editors. *GeneReviews*® [Internet]. Seattle (WA): University of Washington, Seattle; 1993 [cited 2024 Oct 23]. <http://www.ncbi.nlm.nih.gov/books/NBK92946/>.
- Park KC, Krywawych S, Richard E, Desviat LR, Swietach P. Cardiac complications of propionic and other inherited organic acidemias. *Front Cardiovasc Med*. 2020;7:617451.
- Marchuk H, Wang Y, Ladd ZA, Chen X, Zhang G-F. Pathophysiological mechanisms of complications associated with propionic acidemia. *Pharmacol Ther*. 2023;249:108501.
- Takahashi K, Yamanaka S. Induction of pluripotent stem cells from mouse embryonic and adult fibroblast cultures by defined factors. *Cell*. 2006;126:663–76.
- Park I-H, Arora N, Huo H, Maherali N, Ahfeldt T, Shimamura A, et al. Disease-specific induced pluripotent stem cells. *Cell*. 2008;134:877–86.
- Hockemeyer D, Jaenisch R. Induced pluripotent stem cells meet genome editing. *Cell Stem Cell*. 2016;18:573–86.
- Soldner F, Stelzer Y, Shivalila CS, Abraham BJ, Latourelle JC, Barrasa MI, et al. Parkinson-associated risk variant in distal enhancer of α -synuclein modulates target gene expression. *Nature*. 2016;533:95–9.
- Martínez-Pizarro A, Calmels N, Schalk A, Wicker C, Richard E, Desviat LR. Functional analysis of novel variants identified in cis in the PCCB gene in a patient with propionic acidemia. *Gene*. 2024;893:147902.
- Alonso-Barroso E, Brasil S, Briso-Montiano A, Navarrete R, Perez-Cerda C, Ugarte M, et al. Generation and characterization of a human iPSC line from a patient with propionic acidemia due to defects in the PCCA gene. *Stem Cell Res*. 2017;23:173–7.
- Uphoff CC, Drexler HG. Detection of Mycoplasma contamination in cell cultures. *Curr Protoc Mol Biol*. 2014;106:1–14.
- Richard E, Desviat LR, Pérez B, Pérez-Cerdá C, Ugarte M. Three novel splice mutations in the PCCA gene causing identical exon skipping in propionic acidemia patients. *Hum Genet*. 1997;101:93–6.
- Rowe RG, Daley GQ. Induced pluripotent stem cells in disease modelling and drug discovery. *Nat Rev Genet*. 2019;20:377–88.
- Lopez-Marquez A, Alonso-Barroso E, Cerro-Tello G, Bravo-Alonso I, Arribas-Carreira L, Briso-Montiano A, et al. Generation and characterization of a human iPSC line (UAMi004-A) from a patient with propionic acidemia due to defects in the PCCB gene. *Stem Cell Res*. 2019;38:101469.
- Fulgencio-Covian A, Alvarez M, Pepers BA, Lopez-Marquez A, Ugarte M, Perez B, et al. Generation of a gene-corrected human isogenic line (UAMi006-A) from propionic acidemia patient iPSC with an homozygous mutation in the PCCB gene using CRISPR/Cas9 technology. *Stem Cell Res*. 2020;49:102055.
- Desviat LR, Sanchez-Alcudia R, Perez B, Perez-Cerda C, Navarrete R, Vijzelaar R, et al. High frequency of large genomic deletions in the PCCA gene causing propionic acidemia. *Mol Genet Metab*. 2009;96:171–6.
- Alonso-Barroso E, Pérez B, Desviat LR, Richard E. Cardiomyocytes derived from induced pluripotent stem cells as a disease model for propionic acidemia. *Int J Mol Sci*. 2021;22:1161.
- Álvarez M, Ruiz-Sala P, Pérez B, Desviat LR, Richard E. Dysregulated cell homeostasis and miRNAs in human iPSC-derived cardiomyocytes from a propionic acidemia patient with cardiomyopathy. *Int J Mol Sci*. 2023;24:2182.
- Doudna JA, Charpentier E. Genome editing. The new frontier of genome engineering with CRISPR-Cas9. *Science*. 2014;346:1258096.
- Pacesa M, Pelea O, Jinek M. Past, present, and future of CRISPR genome editing technologies. *Cell*. 2024;187:1076–100.
- Haas RH, Marsden DL, Capistrano-Estrada S, Hamilton R, Grafe MR, Wong W, et al. Acute basal ganglia infarction in propionic acidemia. *J Child Neurol*. 1995;10:18–22.
- Wajner M. Neurological manifestations of organic acidurias. *Nat Rev Neurol*. 2019;15:253–71.
- Tristán-Noguero A, Fernández-Carasa I, Calatayud C, Bermejo-Casadesús C, Pons-Espinal M, Colini Baldeschi A, et al. iPSC-based modeling of THD recapitulates disease phenotypes and reveals neuronal malformation. *EMBO Mol Med*. 2023;15:e15847.
- Lancaster MA, Knoblich JA. Organogenesis in a dish: modeling development and disease using organoid technologies. *Science*. 2014;345:1247125.
- Witters P, Debbold E, Crivelly K, Vande Kerckhove K, Corthouts K, Debbold B, et al. Autism in patients with propionic acidemia. *Mol Genet Metab*. 2016;119:317–21.
- de la Bâtie CD, Barbier V, Roda C, Brassier A, Arnoux J-B, Valayannopoulos V, et al. Autism spectrum disorders in propionic acidemia patients. *J Inher Metab Dis*. 2018;41:623–9.
- Zhang W, Zhang M, Xu Z, Yan H, Wang H, Jiang J, et al. Human forebrain organoid-based multi-omics analyses of PCCB as a schizophrenia associated gene linked to GABAergic pathways. *Nat Commun*. 2023;14:5176.

Publisher's Note Springer Nature remains neutral with regard to jurisdictional claims in published maps and institutional affiliations.